MASLOV SHEAR-WAVEFORMS IN HIGHLY ANISOTROPIC SHALES AND IMPLICATIONS FOR SHEAR-WAVE SPLITTING ANALYSES

J. CADDICK,

Department of Earth Sciences[1]

J. M. KENDALL and D. G. RAYMER

Department of Earth Sciences[1]
Western Geophysical[2]

FORMES D'ONDE TRANSVERSALES DE MASLOV DANS LES ARGILES FORTEMENT ANISOTROPES ET IMPLICATIONS DANS LES ANALYSES DE BIRÉFRINGENCE DES ONDES TRANSVERSALES

Les argiles sont les roches sédimentaires les plus répandues dans l'environnement des hydrocarbures, et forment souvent la roche mère et la roche des pièges pétrolifères. En raison de la structure en plaques des grains, les argiles sont généralement anisotropes. Dans le présent article, nous calculons les formes d'onde sismiques pour des argiles fortement anisotropes en employant la théorie asymptotique de Maslov (MAT). Cette théorie est une extension de la théorie classique des rayons qui fournit des formes d'onde valides dans les zones des caustiques (repliement du front d'onde), là où les amplitudes de la théorie des rayons sont instables. La théorie asymptotique des rayons (ART) est basée sur le rayon géométrique ou rayon de Fermat qui relie la source au récepteur. Par contre, la solution de Maslov intègre les données sur des rayons contigüs qui ne sont pas des rayons de Fermat. Les rayons, les temps de propagation, les amplitudes et les sismogrammes synthétiques sont présentés pour trois argiles fortement anisotropes en utilisant un modèle 1D très simple composé d'une argile anisotrope sus-jacente à une argile isotrope. Les formes d'onde ART ne réussissent pas à rendre compte des effets de formes d'onde complexes dues à la triplication. En comparaison, les formes d'onde MAT prévoient les amplitudes régulières aux sommets du front d'onde et les signaux diffractés à partir de ces sommets. Une solution de Maslov qui intègre les contributions des rayons sur une composante unique de lenteur se détériorera si les rayons se focalisent en 3D (sur un point plutôt que le long d'une ligne). Une des argiles testées exhibe cette caustique, et l'intégration sur deux composantes de lenteur est nécessaire pour éliminer la singularisation en amplitude. Nous examinons enfin les effets des triplications du front d'onde sur les rotations de Alford qui sont utilisées pour évaluer la biréfringence des ondes transversales. Dans de tels cas, la rotation trouve avec succès la polarisation de l'onde transversale rapide, mais elle peut s'avérer peu fiable pour l'estimation de l'écart de temps d'arrivée entre les deux ondes transversales.

MASLOV SHEAR-WAVEFORMS IN HIGHLY ANISOTROPIC SHALES AND IMPLICATIONS FOR SHEAR-WAVE SPLITTING ANALYSES

Shales are the most common sedimentary rocks in hydrocarbon environments often forming the source rock and trapping rock for a reservoir. Due to the platey nature of the constituent grains, shales are commonly anisotropic. In this paper we calculate seismic waveforms for highly anisotropic shales using Maslov asymptotic

(1) University of Leeds,
Leeds, LS2 9JT - United Kingdom

(2) 455 London Road, Isleworth
Middlesex, TW7 5AB - United Kingdom

theory (MAT). This theory is an extension of classical ray theory which provides valid waveforms in regions of caustics (wavefront folding) where ray theory amplitudes are unstable. Asymptotic ray theory (ART) is based on the Fermat or geometrical ray which connects the source and receiver. In contrast, the Maslov solution integrates the contributions from neighbouring non-Fermat rays. Raypaths, travel-times, amplitudes and synthetic seismograms are presented for three highly anisotropic shales using a very simple 1D model comprised of an anisotropic shale overlying an isotropic shale. The ART waveforms fail to account for complex waveform effects due to triplications. In comparison, the MAT waveforms predict nonsingular amplitudes at wavefront cusps and it predicts the diffracted signals from these cusps. A Maslov solution which integrates ray contributions over a single slowness component will break down when rays focus in 3D (at a point rather than along a line). One of the tested shales shows such a point caustic and integration over 2 slowness components is required to remove the amplitude singularity. Finally, we examine the effects of wavefront triplications on Alford rotations which are used to estimate shear-wave splitting. In such cases, the rotation successfully finds the fast shear-wave polarization, but it can be unreliable in its estimate of the time separation.

FORMAS DE ONDAS DE CIZALLAMIENTO DE MASLOV EN ESQUISTOS ALTAMENTE ANISOTRÓPICOS Y IMPLICACIONES DEL ANÁLISIS DE DIVISIÒN POR ONDA DE CIZALLAMIENTO

Los esquistos son las rocas sedimentarias más comunes en el entorno de hidrocarburos, formando a menudo la roca fuente y la roca de obturaciòn de un depòsito. Debido al carácter plano de los granos constituyentes, los esquistos son en general anisotròpicos. En este artículo hemos calculado las formas de ondas sísmicas en esquistos altamente anisotròpicos utilizando la teoría asintòtica de Maslov (MAT). Esta teoría es una extensiòn de una teoría de rayos clásica que proporciona formas de ondas válidas en regiones cáusticas (plegamiento de frente de onda), donde las amplitudes teòricas de los rayos son inestables. La teoría asintòtica de rayos (ART) se basa en los rayos Fermat o geométricos que conectan la fuente y el receptor. En contraste, la soluciòn de Maslov integra la contribuciòn de los rayos vecinos no-Fermat. La trayectoria de los rayos, los tiempos de recorrido, la amplitud y los sismogramas sintéticos son presentados para tres esquistos altamente anisotròpicos, utilizando un modelo unidimensional muy simple compuesto por un esquisto anisotròpico que yace por sobre un esquisto isotròpico. Las formas de ondas ART no son capaces de explicar los complejos efectos de formas de onda causados por triplicaciones. En comparaciòn, las formas de ondas MAT predicen amplitudes no-singulares en vértices de frentes de onda y predicen las seòales difractadas de estos vértices. Una soluciòn de Maslov, que integra contribuciones de rayos sobre un componente ˙nico de lentitud, se subdividirá cuando los rayos enfocan en tres dimensiones (en un punto más bien que en una línea). Uno de los esquistos estudiados muestra que un punto cáustico de este tipo y la integraciòn de 2 componentes de lentitud son necesarios para retirar la singularidad de la amplitud. Finalmente, examinamos los efectos de las triplicaciones de frentes de onda sobre rotaciones Alford, utilizadas para estimar la divisiòn por onda de cizallamiento. En tales casos, la rotaciòn encuentra con éxito la polarizaciòn rápida de la onda de cizallamiento; pero puede no ser fiable en su estimaciòn de la separaciòn en el tiempo.

INTRODUCTION

Shales are of fundamental importance to the oil industry as they constitute over 75 percent of the clastic fill in sedimentary basins (Jones and Wang, 1981). They can form the source and trapping rocks for oil and gas accumulations. It is well known that shales behave as transversely-isotropic elastic media due to their finely layered structure (on a scale far smaller than the seismic wavelength), with the symmetry axis perpendicular to the bedding plane. This velocity anisotropy is a function of a number of factors, some of the more important being the kerogen content of the shale and its confining pressure (Vernik and Liu, 1997). The effects of the anisotropy can be quite dramatic and in some cases the *qSV*-wave surfaces show well developed triplications.

Shear-wave and converted-wave surveys are becoming increasingly commonplace and evidence of shear-wave splitting and amplitude anomalies in such data is diagnostic of seismic anisotropy (e.g., Lynn and Thomsen, 1990; Mueller 1991; Kendall and Kendall, 1996). For this reason it is important to understand the effects anisotropy can have on the waveforms. In this study we calculate seismic waveforms for three highly anisotropic shales whose elastic constants are taken from from the studies of Thomsen (1986) and Vernik and Liu (1997).

Asymptotic ray theory (ART) is, in some ways, the simplest method for calculating waveforms, especially in generally anisotropic and inhomogeneous media (Červený, 1972). However, this method breaks down in regions of caustics where rays focus and the wavefronts fold back on themselves. ART predicts infinitely large amplitudes at the wavefront cusps and fails to predict the diffracted signals from these cusps. Ray theory is only concerned with the Fermat or geometrical ray which connects the source and receiver. Maslov asymptotic theory (MAT) is less local in that it sums the contributions to the receiver waveform from neighbouring non-Fermat rays. A consequence of the Maslov formalism is that it provides a valid waveform solution near caustics. Maslov (1965) first developed the theory as a semi-classical solution to the Schrödinger wave equation. The technique was introduced to seismology by Chapman and Drummond (1982) and Kendall and Thomson (1993) verified the method for the anisotropic case. Huang *et al.* (1998) demonstrated the accuracy of MAT seismograms

through comparisons with finite-difference seismograms. The Maslov approach is much faster than finite difference techniques, as ray tracing is the time limiting step in the calculation.

The model we adopt for this study is very simple, consisting of an anisotropic shale overlying a isotropic shale half-space. Rays and their amplitudes are traced through these models using the ray tracer ATRAK (Guest and Kendall, 1993). Ray theory seismograms are compared with the Maslov seismograms, highlighting the failure of ray theory especially in the neighbourhood of triplications. Maslov synthetics are generated via an integration over one component of the horizontal slowness. One of the shales exhibits ray focusing at a point caustic rather than the more common fold singularity or line caustic. In such cases the 1D integral solution breaks down and we show how stable amplitudes are achieved via an integral solution over both components of the horizontal slowness. Whilst the integral is in principle easy to compute numerically, few examples have ever been calculated (Kendall and Thomson, 1993; Caddick, 1997). The final part of the paper examines the effect of wavefront triplications on Alford rotations (Alford, 1986) which are used to estimate shear-wave splitting in data.

1 SHALES AND ANISOTROPY

Shale is a fine grained sedimentary rock usually consisting of both silt and clay. It is noted for its fissility where the associated splitting takes place along the surfaces of the laminations within the shale. Typically shales undergo pronounced compaction as they lithify. Pressure from overlying material reduces the overall volume and packs the sediment grains together as water is squeezed from the pores. Clay minerals become oriented parallel to one another and lie orthogonal to the applied pressure. Shales are generally impermeable and are of medium to low porosity.

An especially important property of shales is that they are transversely isotropic with velocities in the bedding plane faster than velocities along the vertical axis of symmetry. Jones and Wang (1981) studied Cretaceous shales from the Williston basin at depths of 3200 ft/975 m and 5000 ft/1524 m (the 5000 ft shale is actually shale B in this study). They found the 5000 ft shale with 11% porosity to be much more anisotropic (over 20% in v_p) than the 3200 ft shale with 16% porosity (12% in V_p). This phenomena has been attributed to an increasing preferred orientation of mineral grains with increasing bulk density (Kaarsberg, 1959). Micro-photographs of the shales studied by Jones and Wang (1981) confirm this.

Vernik and Liu (1997) suggest that the strong intrinsic velocity anisotropy of shales is associated with laminated/lenticular texture of clay aggregates "floating" in a continuous, anisotropic kerogen network. They find that the Thomsen (1986) parameter, ε, increases with kerogen content, especially for black shales with moderate clay content. The magnitude of intrinsic anisotropy is particularly high in compacted, low-porosity black shales compared to their high porosity equivalents. The strong intrinsic shale anisotropy is also enhanced by bedding-parallel microcracks. This is in agreement with Vernik and Nur (1992), who found that microcracks inferred from ultrasonic velocity measurements occur only in mature shales. Similarly, they relate the anisotropy to the kerogen content, microstructure and maturation level of the shale.

Three highly anisotropic shales have been chosen for our modelling (Table 1). The first shale is taken from the database in Appendix A of Vernik and Liu (1997). It is from a depth of 12507 ft/3012 m in the Bazhenov formation and will be referred to as shale A. It is of particular interest because despite the large Thomsen parameters, it does not exhibit any shear-wavefront folding. Two other shales were chosen from Thomsen (1986): the first, here referred to as shale B, is listed as "shale (5000)" and the second is the "Mesaverde (5501) clay shale", which will be referred to as shale C. Both of these shales exhibit shear-wavefront folding.

TABLE 1

Measured vertical velocities and Thomsen parameters for shale A (from Vernik and Lui, 1997) and shales B and C (from Thomsen, 1986)

	v_p (m/s)	v_s (m/s)	ρ (kg/m^3)	ε	γ	δ
A	3300	2300	2500	0.58	0.39	0.84
B	3377	1490	2420	0.200	0.510	– 0.075
C	3928	2055	2590	0.334	0.575	0.730

2 THEORY

2.1 Asymptotic Ray Theory

Ray theory provides an asymptotically accurate estimate of the first motions of transient waveforms.

That is, the higher the frequency, the more accurately the approximation satisfies the wave equation. A big advantage of ART is that it provides a computationally quick way of tracking wavefronts and their amplitudes through 3D inhomogeneous anisotropic media. It is also a useful interpretation tool in that it allows the user to monitor a given wavetype as it propagates through a model. There are, though, certain interesting cases where ART beaks down. For example, near caustics, rays focus and cross and the wavefront folds over on itself producing traveltime triplications. Rays can be traced through such regions without difficulty, but the amplitudes of the rays at and near the cusps of the triplications will be overestimated. Also, as with any diffraction, ray theory fails to estimate the non-geometrical signals which decay away from the cusps.

The following outlines ART for 3D anisotropic media. Details can be found in Červený (1972), Gajewski and Pšencík (1987) or Kendall and Thomson (1989). Consider the wave equation expressed in the frequency domain for an inhomogeneous anisotropic medium:

$$\frac{\partial}{\partial x_i}\left(C_{ijkl} \frac{\partial u_k}{\partial x_1} \right) + \omega^2 \rho u_j = 0 \qquad (1)$$

where

u_i is the particle displacement,
C_{ijkl} is the tensor of elastic parameters,
ρ is the density,
x_i are the spatial coordinates and
ω is the frequency.

A solution is sought in the form of an asymptotic series and the zeroth-order ART solution is of the form:

$$u_k(x,\omega) \cong A g_k e^{i\omega t} \qquad (2)$$

where

t is the phase function,
A is the scalar amplitude and
g_k is the particle motion.

Substituting (2) into (1) and collecting coefficients of powers of frequency, ω, leads to the well known eikonal and transport equations. The eikonal equation can be solved using the method of characteristics to generate a set of ray equations, which are in turn used to derive the geometrical spreading equations (for a discussion of this see Kendall and Thomson (1989)). These equations are used to track the time, location and slowness of a wavefront and lead to calculations of the wavefront amplitudes.

The amplitude is obtained from the transport equation. It can be shown that:

$$A(x_1, x_2, x_3) = C_o \left| \rho J \right|^{-1/2} \qquad (3)$$

where:

$$J = \left(\frac{\partial (x_1, x_2, x_3)}{\partial (\alpha_1, \alpha_2, \alpha_3)} \right) \qquad (4)$$

is the Jacobian of the geometrical spreading terms and C_0 is a constant of integration. The terms α_i are a set of initial conditions which define the ray. For example, Červený (1972) uses the ray take-off angles and the time along the ray for α_i. At caustics, rays focus and the geometrical spreading term, J, equals zero. Therefore, the amplitudes, A, at caustics are erroneously predicted to be infinitely large.

2.2 1D Maslov Asympotic Theory

Due to the band-limited nature of seismic data, a bundle of rays around the geometrical ray will affect the waveform at a given receiver. The cross-sectional size of this bundle is related to the Fresnel zone which is frequency dependent and controls the wavefield resolution. As with other transform methods (e.g., WKBJ seismograms (Chapman, 1978)), the Maslov solution is less local than ART as it sums the contribution of rays in the neighbourhood of the Fermat ray. Each ray is identified with the components of a slowness vector (p_1, p_2, p_3) and the summation can be over any number of these components.

With 1D integration, for example over the p_1 component, the Maslov asymptotic solution is of the form:

$$u_k(x,\omega) \cong \left(\frac{i\omega}{2\pi} \right)^{1/2} \int B g_k e^{i\omega\theta} \, dp_1 \qquad (5)$$

where

$\theta = \theta\ (p_1, x_2, x_3)$ is the Maslov phase, and
$B = B\ (p_1, x_2, x_3)$ is the Maslov amplitude.

Equation (5) can be substituted into (1) and a new set of ray and geometrical spreading equations can be calculated, but in practice this is not required. The Maslov phase, θ, is simply calculated from the ray tracing results (see, for example, Chapman and Drummond (1982) or Guest and Kendall (1993)).

The Maslov amplitude is easily calculated from the geometrical spreading terms and has the form:

$$B(p_1, x_2, x_3) = C_0 \left| \rho \tilde{J} \right|^{-1/2} \tag{6}$$

where:

$$\tilde{J} = \left(\frac{\partial (p_1, x_2, x_3)}{\partial (\alpha_1, \alpha_2, \alpha_3)} \right) = J \left(\frac{\partial p_1}{\partial x_1} \right) \tag{7}$$

As a ray approaches a caustic the Jacobian J shrinks to zero whilst the term $\frac{\partial p_1}{\partial x_1}$ goes to infinity rendering the product of he terms nonsingular. Therefore, the Maslov amplitude is nonsingular at a caustic. More generally speaking, this is a consequence of Liouville's theorem which states that there will always be a set of nine geometrical-spreading terms (the partial derivatives) whose determinant is non-zero (Thomson and Chapman, 1985). The Maslov approach overcomes the ray theory singularities by using a different Jacobian. There may also be singularities in the Jacobian, $\tilde{\boldsymbol{J}}$, in which case a different Jacobian must be used. This occurs, for example, at point caustics where the rays focus at a point.

2.3 2D Maslov Theory

To solve the problem of singularities at point caustics an integral over two slowness components is required. Despite being relatively simple to compute, examples involving 2D Maslov solutions are not commonplace and few numerical examples have been calculated. The resulting 2D Maslov solution is of the form:

$$u_k(x, \omega) \cong \left(\frac{i\omega}{2\pi} \right) \iint D g_k \, e^{i\omega\Theta} \, \mathrm{d}p_1 \, \mathrm{d}p_2 \tag{8}$$

where:

$$D(p_1, p_2, x_3) = C_0 \left| \rho \tilde{\tilde{J}} \right|^{-1/2} \tag{9}$$

and

$$\tilde{\tilde{J}} = \left(\frac{\partial (p_1, p_2, x_3)}{\partial (\alpha_1, \alpha_2, \alpha_3)} \right) \tag{10}$$

The Maslov phase for the 2D integral case, $\Theta(p_1, p_2, x_3)$, is again easily calculated from the ray tracing results and the Maslov amplitude $D(p_1, p_2, x_3)$, is calculated from the standard geometrical spreading equations. The amplitude is now stable in the vicinity of point caustics as the Jacobian, $\tilde{\tilde{J}}(p_1, p_2, x_3)$, will be nonsingular.

3 RESULTS

In this section we generate ART and Maslov seismograms for a simple model of an anisotropic shale overlying an isotropic halfspace (Fig. 1). The vertical *P*- and *S*-velocities are chosen to be constant throughout the model. There is, though, a discontinuity in the horizontal velocity at the interface due to the anisotropy in the overlying layer. We assume a non-physical point source buried in the isotropic region at a depth of 1 km which generates *P, SV* and *SH* energy equally in all directions. Synthetic seismograms are calculated for a range of offsets using both ray theory (2) and the 1D Maslov integral solution (5). Details of the numerical implementation of the theory can be found in Guest and Kendall (1993). The first step is to trace rays through each of the models. Only the *qSV*-wavefronts show triplications in these examples, therefore, in the interest of brevity, we only show waveforms for the *qSV*-waves. Caddick (1997) shows that the ART and MAT waveforms for both the *qP*- and *qSH*-waves in this model are in good agreement with each other, but significant differences occur for the *qSV*-waveforms.

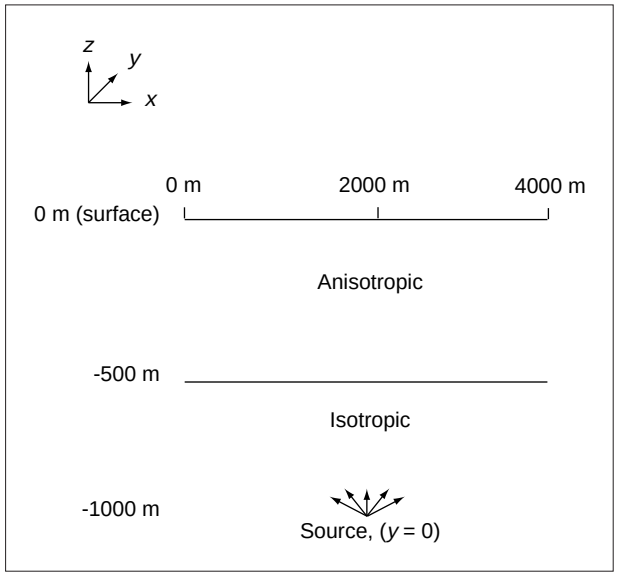

Figure 1

Schematic representation of the model. A 500 m thick anisotropic layer overlies an isotropic halfspace and the source is 1000 m deep at x = 2000 m.

3.1 Shale A

The slowness and wave surfaces for shale A (Table 1) are shown in Figure 2a. This illustrates the degree of anisotropy in the upper layer of the model. Clearly there is shear-wave splitting, but there is no wavefront folding on any of the 3 wave surfaces (*qP*-waves never e ing in homogeneous media).

In order to calculate the ART and MAT waveforms, 100 rays are traced between 1000 m and 3000 m. The ART waveforms are calculated at receivers every 200 m through interpolation. This avoids the singularity in the ray equations along the vertical axis. Figure 2b, shows the ray paths, traveltimes and ART amplitudes for the *qSV*- and *qSH*-waves.

Figure 3 shows the ART and 1D MAT waveforms for this model. The synthetics have been convolved with a smoothed delta function with a centre frequency of 25 Hz and a sampling rate of 5 ms. Convolution with a ricker wavelet, for example, would produce waveforms which are more realistic, but a delta function has been used for simplicity in comparisons. The synthetics differ at the receivers near 2 km where the ART solution overestimates the amplitudes. This is due to the ray focusing directly above the source (Fig. 2b). Ray theory assumes that the wavefront has a constant Gaussian curvature which is clearly not the case in this example. The wavefront has much higher curvature near the area of ray focusing than it does at far offsets. As a result, the waveforms are less sensitive to the contributions from neighbouring rays as they are more removed in time from the geometrical arrivals. This illustrates how the Maslov synthetics can give a more accurate solution even in situations where there are no triplications.

The Maslov synthetics show low amplitude endpoint signals. These numerical artefacts are due to the truncation of the slowness integral (5) used to calculate the waveforms. For a complete description of these artefacts see Thomson and Chapman (1986). The endpoint signals are easily predicted as they move out with the slownesses of the truncation rays (± 0.00048 s/m in Figure 3).

3.2 Shale B

The Thomsen parameters for shale B are shown in Table 1 and vertical cross-sections of the slowness and

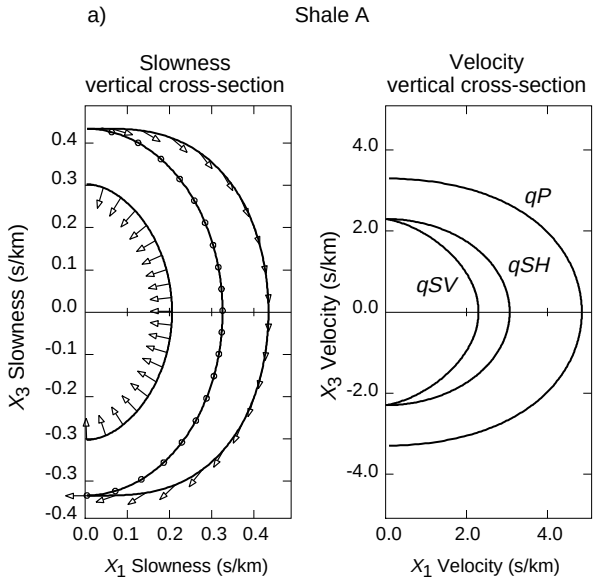

Figure 2a

Vertical section of the slowness (left) and wave or group-velocity (right) surfaces for shale A. Polarizations are illustrated with arrows on the slowness surfaces.

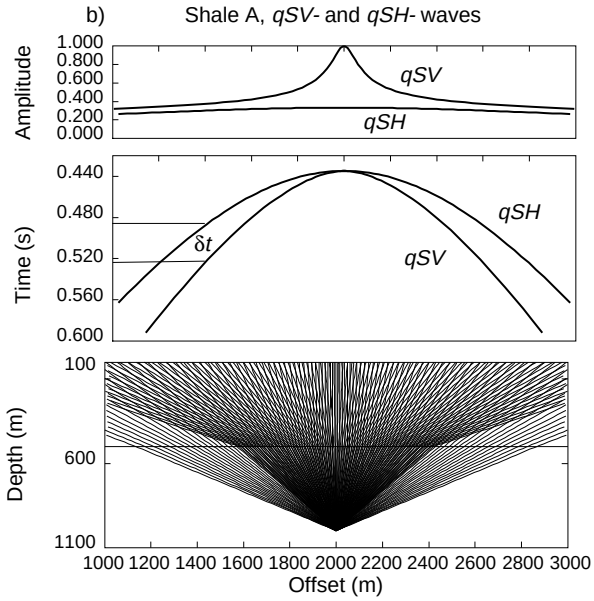

Figure 2b

Raypaths, traveltimes and ART amplitudes for *qSV*- and *qSH*-waves in the shale A model.

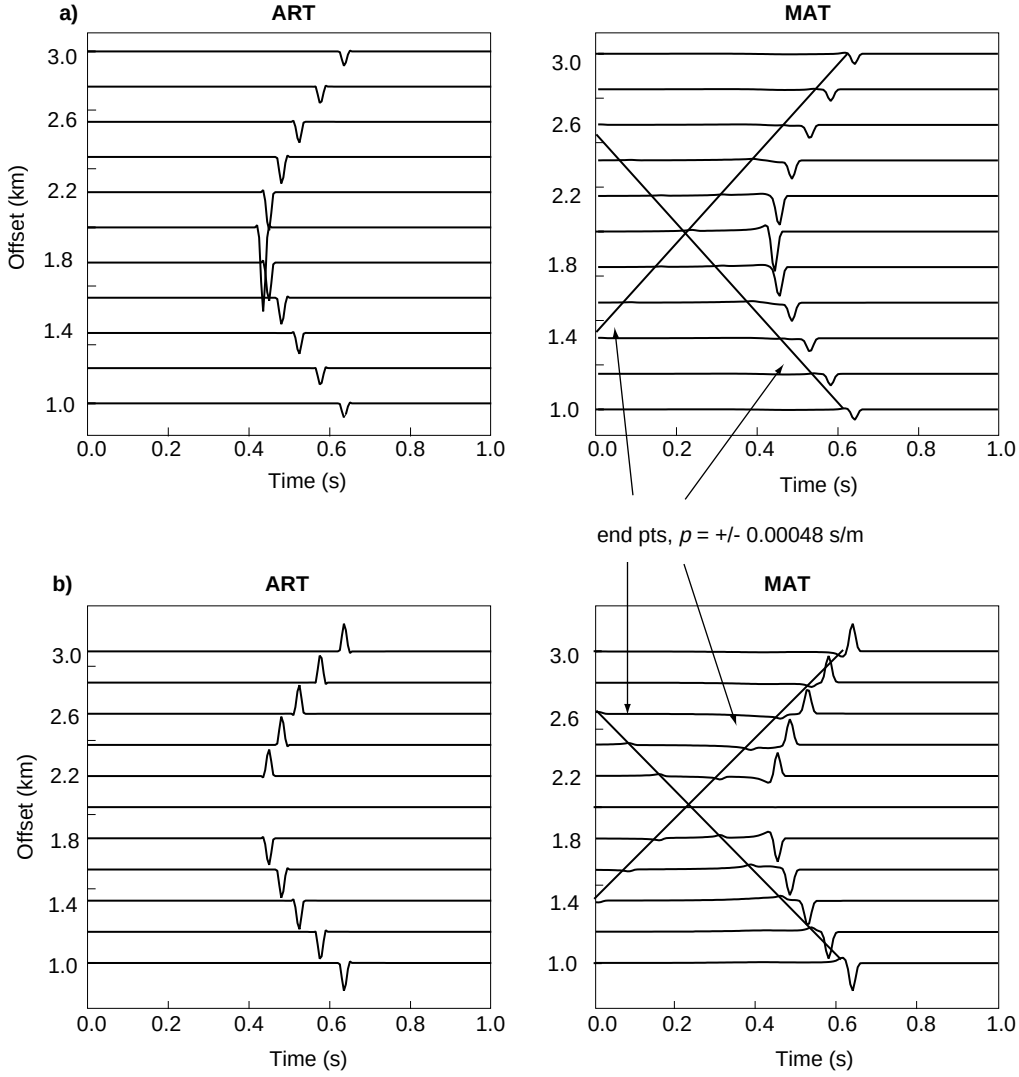

Figure 3

ART (left) and MAT (right) *qSV*- seismograms for the shale A model. The top shows the horizontal component waveforms and the bottom shows the vertical component waveforms. Signals associated with endpoints in the Maslov integral are indicated on the MAT waveforms.

wave surfaces are shown in Figure 4a. The *qSV*-wavefront shows two well developed triplications, whilst the *qSH*-and *qP*-wave surfaces have simple geometries. The raypaths (Fig. 4b) show the *qSV*-rays focusing at two caustics and forming two travel-time triplications at the surface. The singularities in the ART amplitudes at the cusps of the traveltime triplications are clearly visible.

Figure 5 shows how different the ART synthetics are from the MAT seismograms in the vicinity of the triplications. The wavefront folding leads to 3 arrivals. The 2 forward branches of the triplication will be delta functions, and the reverse branch will be the Hilbert transform of a delta function. The individual arrivals cannot be discriminated in the waveforms as they are separated by only a few milliseconds. The large ART amplitudes at the triplications dominate the ray theory results. The MAT seismograms show an increase in amplitude due to ray focusing near the caustics, but the amplitudes are more smoothly varying through the region. Furthermore, the Maslov results show the diffractions from traveltime cusps (indicated in Figure 5).

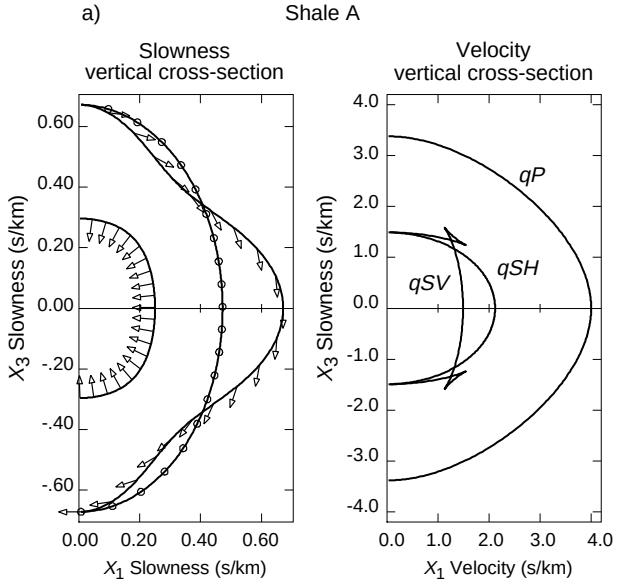

Figure 4a

Vertical section of the slowness (left) and wave or group-velocity (right) surfaces for shale B. Polarizations are illustrated with arrows on the slowness surfaces.

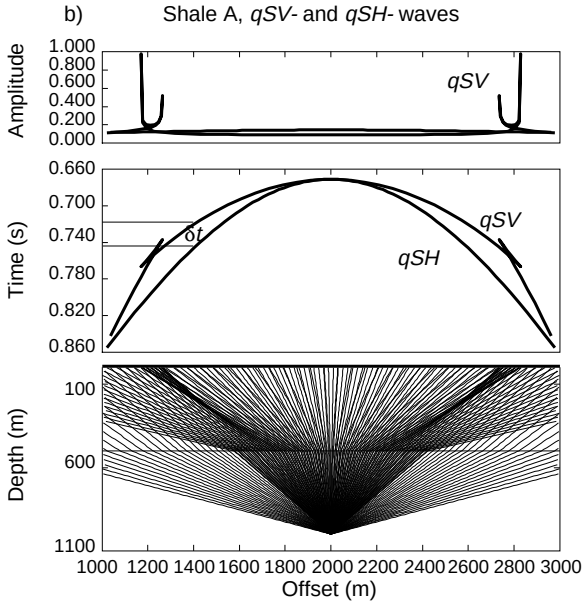

Figure 4b

Raypaths, traveltimes and ART amplitudes for *qSV*- and *qSH*-waves in the shale B model. Note the traveltime triplication and amplitude singularities on the *qSV*-arrivals near 1200 m and 2800 m.

Ray theory does not predict these diffractions as they are not geometrical arrivals. Through comparisons with finite difference waveforms, Huang *et al.* (1998) show that these signals can be accurately predicted using Maslov theory. Although it should be noted that, like ray theory, the Maslov approach is still a high-frequency approximation and at low frequencies the Maslov seismograms will overestimate the strength of the diffractions (Huang *et al.*, 1998). It is possible that these signals are slightly overestimated in Figure 5. A final comment is that the integration endpoint signals have little effect on the MAT seismograms for this model.

3.3 Shale C

The third example, shale C (Table 1), shows triplications along the coordinate axes (Fig. 6a). This produces ray focusing and a traveltime triplication in the region directly above the source (Fig. 6b). In addition to the ART amplitude singularities at the cusps of the triplication, there is also a singularity on the ray which travels vertically upwards from the source (this is discussed in more detail in the next section). An interesting feature in the propagation of *qSV*-waves through this model is that the raypaths between 1600 m and 2400 m, and hence the group velocities, change their direction of lateral motion as they cross the model interface. For example, in the region around 1800 m, the rays switch from moving towards the left to moving toward the right. Snell's law is satisfied and it can be shown that the wavefront normals, and hence the phase velocities, retain their leftward direction. This is an example of where the group and phase velocities are dramatically different in direction.

The ART and MAT waveforms for this model are very different (Fig. 7), and unfortunately, both are in error. The 1D-integral Maslov solution overcomes the singularities at the wavefront cusps, but it fails to overcome the singularity at 2000 m. This is due to the rays focusing in 3D directly above the source. The resulting point caustic renders both the ART and 1D-MAT Jacobians (Eqs (4) and (7)) singular. The Maslov seismograms show diffractions from the traveltime cusps which are correct, but they also show an erroneous diffraction from the point singularity. This is an example where a 2D Maslov integral is required.

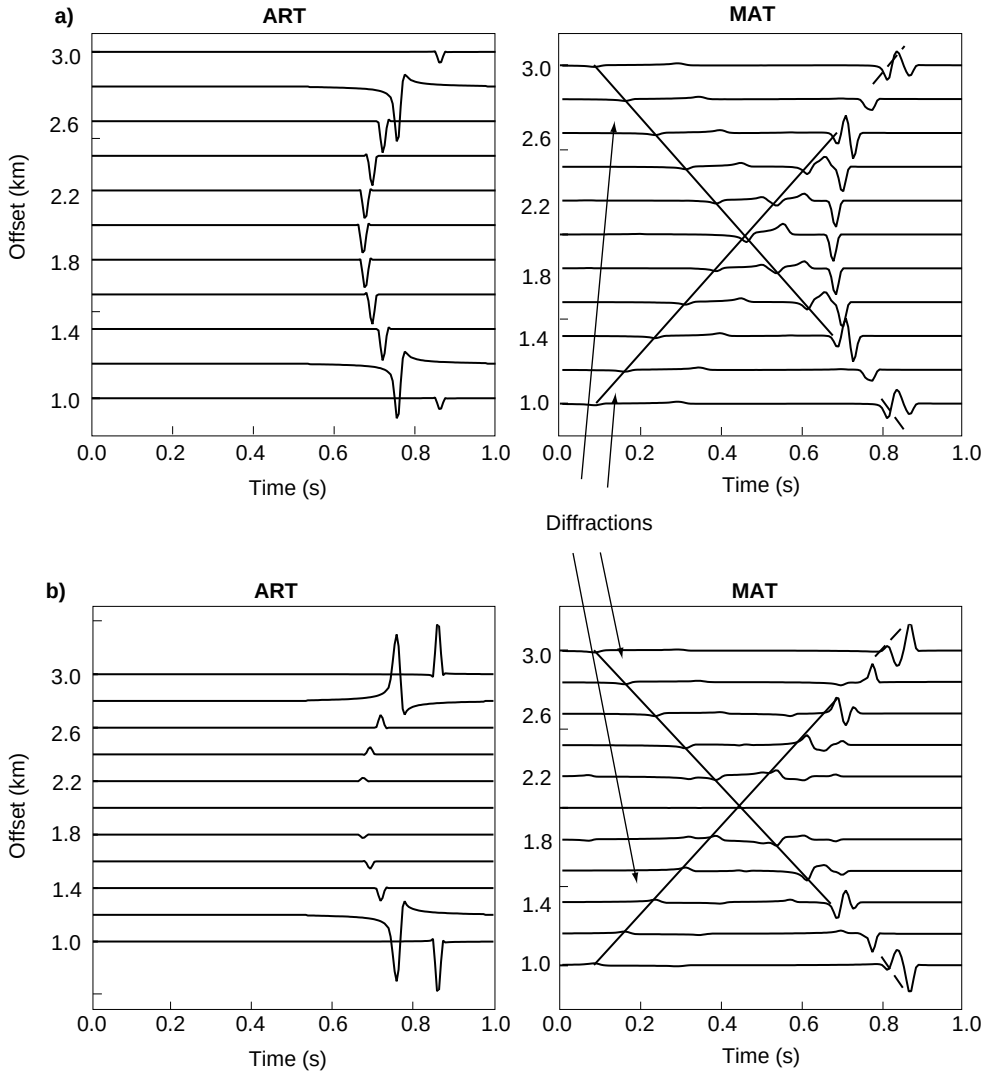

Figure 5.

ART (left) and MAT (right) *qSV*- seismograms for the shale B model. The top shows the horizontal component waveforms and the bottom shows the vertical component waveforms. The diffractions from the traveltime triplications are shown for the MAT waveforms.

3.4 Discussion of the Amplitude Singularities

Comparisons of the ART and MAT amplitudes for the folded *qSV*-wavefronts in the shale models B and C are shown in Figure 8. Figure 8a shows the singularities in the ray theory amplitudes at the wavefront cusps in the vicinity of 1200 m in the shale B model. The wavefront is simply folded in this example and the 1D-integral Maslov amplitude (6) is nonsingular, varying smoothly through this region. The situation is a more complicated in the shale C model. Figure 8b shows 3 singularities in the ART amplitudes. There is a wavefront fold roughly 35 m from the receiver directly above the source (at 2 km). The 1D Maslov amplitude (6) removes this singularity as expected. There is also a point caustic at 2km, where the wavefront collapses to a point and the 1D Maslov solution is singular. Figure 8c shows that the 2D Maslov amplitude (9) is non-singular at both types of caustics and is smoothly varying through the entire region. Caddick (1997) presents the resulting 2D Maslov waveforms for this example.

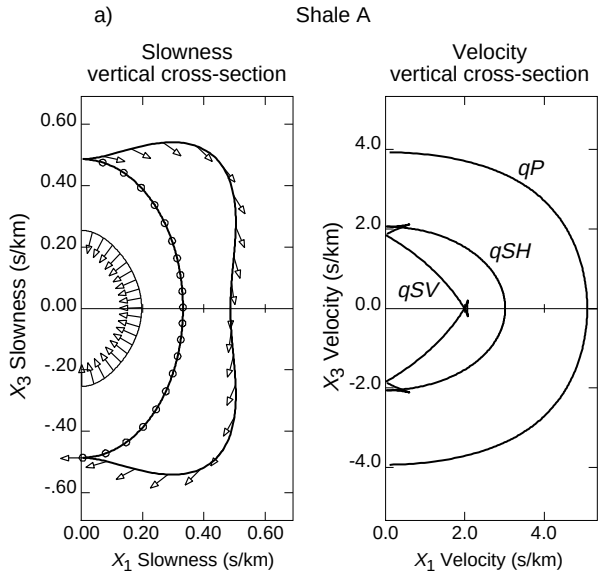

Figure 6a

Vertical section of the slowness (left) and wave or group-velocity (right) surfaces for shale C. Polarizations are illustrated with arrows on the slowness surfaces.

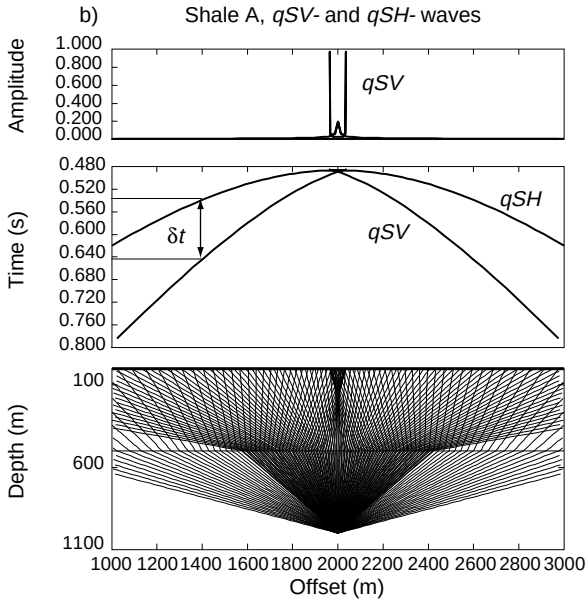

Figure 6b

Raypaths, traveltimes and ART amplitudes for *qSV*- and *qSH*-waves in the Shale C model. Note the traveltime triplication and amplitude singularities on the *qSV*-arrivals near 2000 m.

4 ALFORD ROTATIONS

In general, a shear-wave incident on an anisotropic medium will be split into two orthogonally polarized shear-waves which travel with different velocities. A 3-component receiver will record some combination of these fast and slow shear-wave arrivals. The Alford rotation (Alford, 1986) is a mathematical algorithm which rotates the components to find the fast shear-wave polarization, ϕ, and the delay time, δt, between the two shear-waves. The Alford rotation is not needed in the case of transverse isotropy with a vertical symmetry axis (VTI) as the fast and slow shear waves are decoupled regardless of the receiver orientation at the surface (note this is not the case for receivers in a borehole). In this section we consider the case where the shale is dipping which means there will be *qSV*- and *qSH*-energy on both the inline and crossline receiver components.

In order to test the rotation analysis we assume that the arrival at 1400 m for the 3 shale models is a vertically travelling ray. This is equivalent to having the shales dipping ~ 30° from the horizontal. The 1400 m offset waveforms are then rotated 45° which yields both *qSV*- and *qSH*-energy on the inline and crossline components. The Alford rotation is then applied to see if it correctly estimates the splitting parameters, ϕ and δt.

In this section we are interested in testing the Alford algorithm for the case where the fast and slow shear-waveforms are substantially different in character. This is the case for the model with shale B in the top layer. At 1400 m the *qSV*-arrival is near the triplication and the resulting waveform is quite different from the *qSH*-waveform. The first step in the analysis is to rotate the horizontal components to find the fast and slow shear-waves. In practice the splitting parameters are found through a grid search over a range of values for δt and ϕ. Figure 9 shows the results of the analyses. The fast and slow shear-wave are successfully found for this example, despite the differences in waveforms. The estimated splitting parameters are δt = 24 ms ± 3 ms and ϕ = 47° ± 7°, which agree well with the actual values of 25 ms and 45°. The uncertainties in the estimates are due to the differences in the waveform shape. The estimate of ϕ is robust, but the estimate of δt. is sometimes erroneous. Experiments with more complicated, and perhaps more realistic, source waveforms showed that the algorithm sometimes aligns the wrong peak in the *qSV*-waveform. Further investigation of this is required.

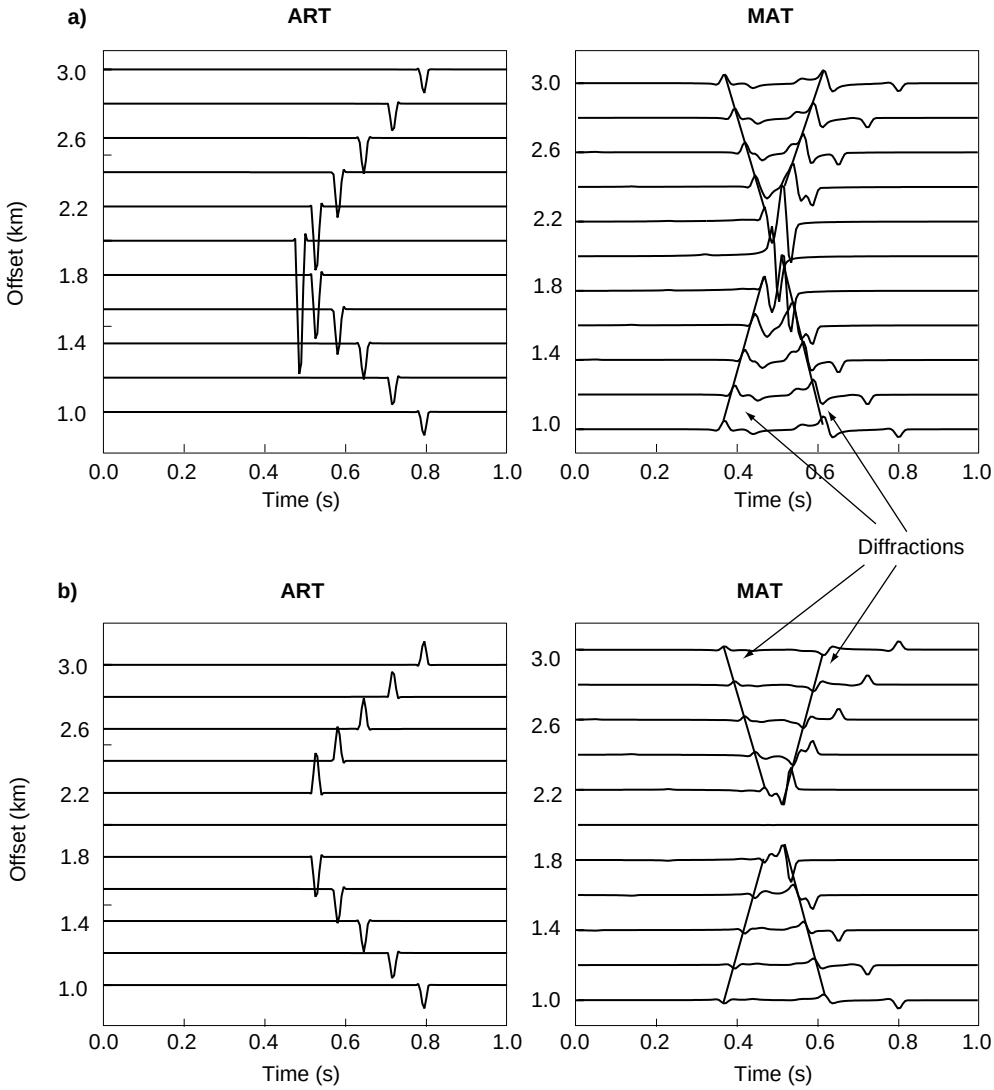

Figure 7

ART (left) and MAT (right) *qSV*-seismograms for the shale C model. The top shows the horizontal component waveforms and the bottom shows the vertical component waveforms. The diffractions from the traveltime triplications and the diffractions from the singularity in the 1D Maslov solution are shown on the MAT waveforms.

Caddick (1997) shows examples for each of the models. Not surprisingly, the Alford rotation correctly estimates the splitting parameters for the shale A and C models where the waveforms are very similar in the region around 1400 m.

5 DISCUSSION

Wave propagation effects in our 1D models with highly anisotropic shales can be quite complicated despite the simplicity of the models. It is well known that ART breaks down in the vicinity of caustics predicting infinitely large amplitudes at the cusps of traveltime triplications and failing to predict the diffractions from these cusps. Our examples show how MAT predicts valid waveforms in the vicinity of caustics. A more subtle observation is that the ART provides a poor estimate of amplitudes in regions of sharp changes in the wavefront curvature. Therefore, Maslov theory should be used in regions of strong ray focusing or defocusing. A case where a Maslov 2D

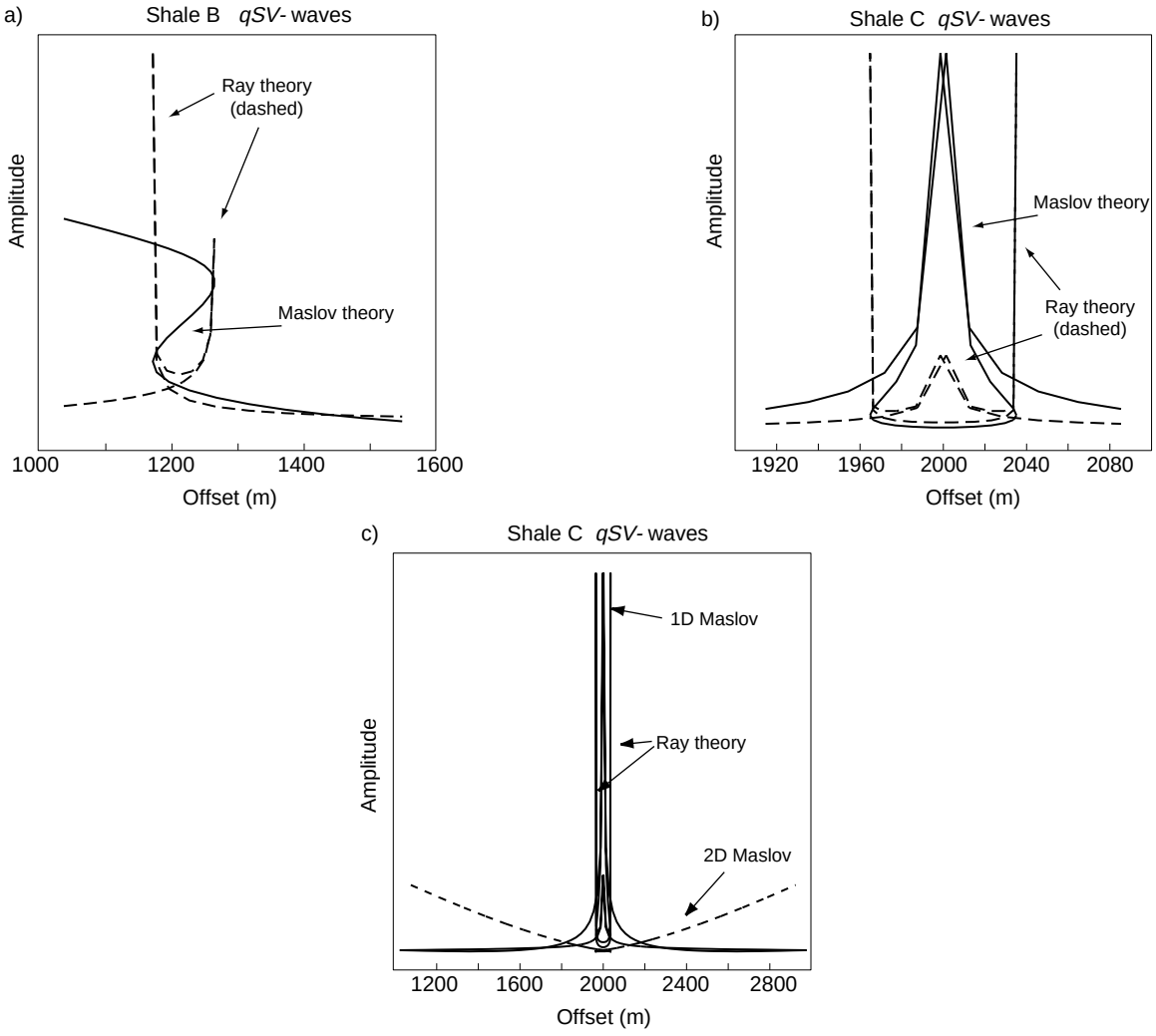

Figure 8

Comparisons of the ART and MAT amplitudes in the vicinity of shear-wave triplications.

(a) The amplitudes in the vicinity of the triplication for the shale B model.

(b) The amplitudes in the vicinity of the point caustic in the shale C model. Note the 3 singularities in the ART amplitudes and the 1 singularity in the 1D Maslov theory.

(c) Note that the smoothly varying 2D Maslov solution (dashed line) has no singularities.

integral solution is required occurred for one of the shale models with a point caustic (the wavefront collapses to a point).

While one S-wavefront may exhibit folding, the other generally does not, yielding very different waveforms for the slow and fast S-waves. This has obvious implications for shear-wave splitting analyses where estimates of δt. implicitly assume each waveform is similar in shape. Experiments with Maslov waveforms suggest that in such cases conventional splitting analyses may give unreliable estimates of the delay times, but it still does a reasonable job of estimating the polarization directions.

ACKNOWLEDGMENTS

Two anonymous reviewers are thanked for helpful comments which improved the paper. We acknowledge the hard work of Jean Arnaud for organizing the *8th IWSA* and Patrick Rasolofosaon for editing this volume. J. Caddick received MSc support from *NERC-UK*.

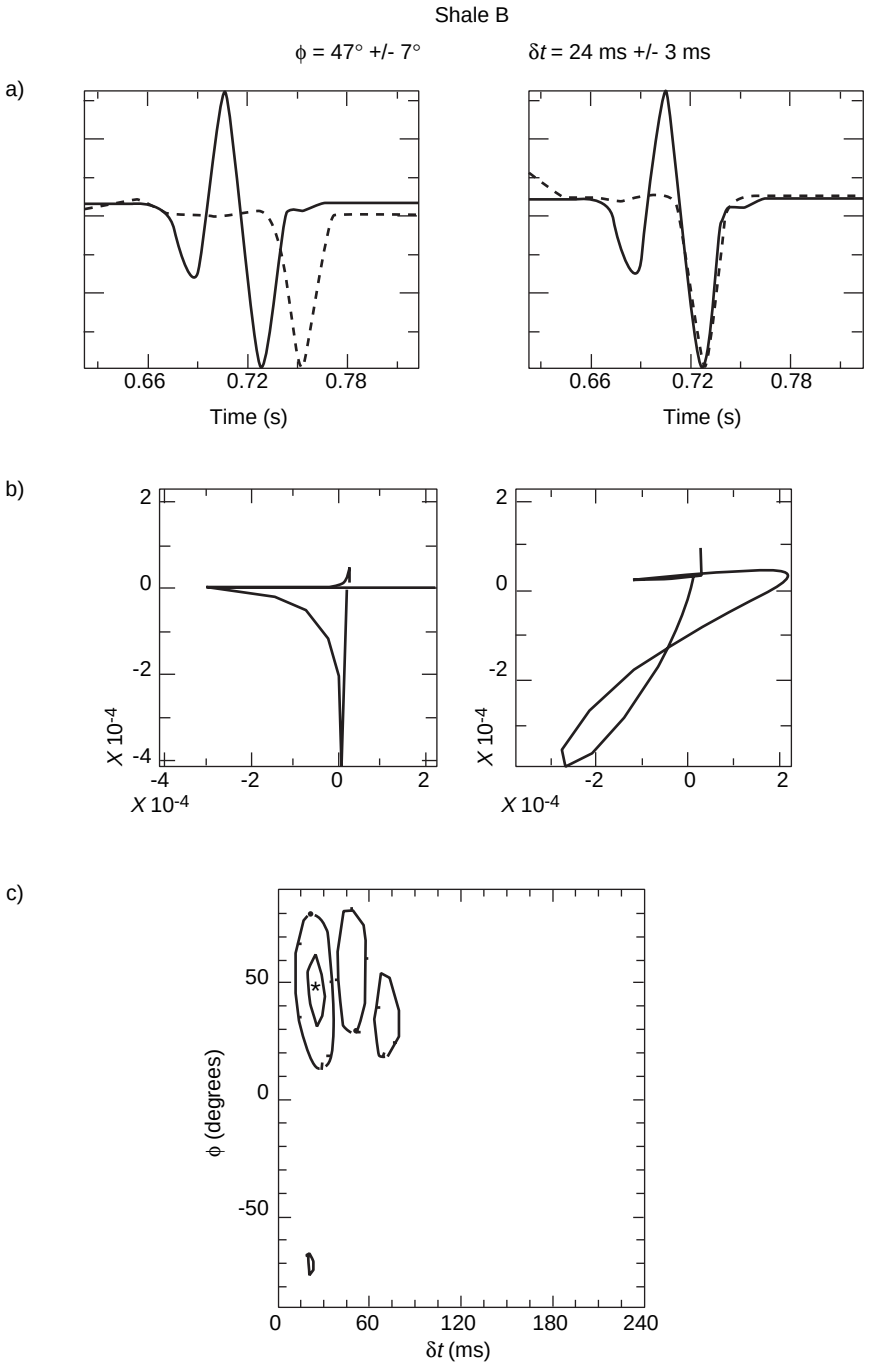

Figure 9

An illustration of the splitting analyses:

(a) The fast and slow shear-waveforms are isolated through rotations of the horizontal components. The left shows the waveforms before correcting for the splitting, whilst the right shows the time-shifted waveforms.

(b) The particle motions before and after the splitting correction.

(c) Contours of the best estimate of shear-wave time separation, δt, and fast shear-wave polarization, ϕ. The innermost contour around the "*" marks the 95% confidence level based on a statistical *F*-test.

REFERENCES

Alford R.M.(1986) Shear data in the presence of azimuthal anisotropy. *56th Ann. Internat. Mtg. (Houston), SEG,* Expanded Abstracts, Dilley Texas, 476-479.

Caddick J. (1997) Maslov seismic synthetic waveforms for strongly anisotropic shales and implications for shear-wave splitting analyses. *MSc. Thesis,* University of Leeds.

Červený V. (1972) Seismic rays and ray intensities in inhomogeneous anisotropic media. *Geophys. J. R. Astr. Soc*., 29, 1-13.
Chapman C.H. (1978). A new method for computing synthetic seismograms. *Geophys. J. R. Astr. Soc.*, 16, 81-85.

Chapman C.H. and Drummond R.(1982) Body-wave seismograms in inhomogeneous media using Maslov asymptotic theory. *Bull. Seism. Soc. Am. ,* 72, S277-S317.

Gajewski D. and Pšencík I. (1987) Computation of high-frequency seismic wavefields in 3-D laterally inhomogeneous anisotropic media. *Geophys. J. R. Astr. Soc.*, 91, 383-411.

Guest W.S. and Kendall J.M. (1993) Modelling seismic waveforms in anisotropic inhomogeneous media using ray and Maslov asymptotic theory: Applications to exploration seismology. *Canadian J. Expl. Geophys.*, 29, 78-92.

Huang X., Kendall J.M., Thomson C.J. and West G.F. (1998) A comparison of the Maslov integral seismogram and the finite-difference method. *Geophys. J. Int.,* 132, 584-594.

Jones L.E A. and Wang H.F. (1981) Ultrasonic Velocities in Cretaceous shales from the Williston basin. *Geophysics*, 46, 288-297.

Kaarsberg E.A (1959) Introductory studies of natural and artificial argillaceous aggregates by sound propagation and X-ray diffraction methods. *J. Geol.,* 67, 447-472.

Kendall J.M. and Thomsen C.J (1989) A comment on the form of the geometrical spreading equations, with some numerical examples of seismic ray tracing in inhomogeneous, anisotropic media. *Geophys. J. Int.,* 99, 401-413.

Kendall J.M. and Thomsen C.J. (1993) Maslov ray-summation, pseudocaustics, Lagrangian equivalence and transient seismic waveforms. *Geophys. J. Int.,* 113, 186-214.

Kendall R.R. and Kendall J.M. (1996) Shear-wave amplitude anomalies in south-central Wyoming. *The Leading Edge*, 15, 913-920.

Lynn H.B. and Thomsen L.A (1990) Reflection shear-wave data collected near the principle axes of azimuthal anisotropy. *Geophysics*, 55, 147-156.

Maslov P. (1965) *Theory of Perturbations and Asymptotic Methods* (in Russian), Izd., MGU, Moscow.

Mueller M.C. (1991) Prediction of lateral variability in fracture intensity using multicomponent shear-wave surface seismic as a precursor to horizontal drilling in the Austin Chalk. *Geophys. J. Int.,* 107, 409-415.

Thomsen L.A. (1986) Weak elastic anisotropy. *Geophysics,* 51, 1954-1966.

Thomson C.J. and Chapman C.H.(1985) An introduction to Maslov's asymptotic method. *Geophys. J.R. Astr. Soc.*, 83, 143-168.

Thomson C.J. and Chapman C.H. (1986) Endpoint contributions to synthetic seismograms. *Geophys. J.R. Astr. Soc.*, 87, 285-294.

Vernik L. and Nur A. (1992) Ultrasonic velocity and anisotropy of hydrocarbon source rocks. *Geophysics*, 57, 727-735.

Vernik L. and Lui X. (1997) Velocity Anisotropy in shales: A petrophysical study. *Geophysics*, 62, 521-532.

Final manuscript received in July 1998